Global factors that determine the maximum disparity for seeing cyclopean surface shape

Lynn R. Ziegler *, Robert F. Hess, Fred A.A. Kingdom

McGill Vision Research Unit, Department of Ophthalmology, McGill University, 687 Pine Avenue West, H4-14, Montreal, Québec, Canada, H3A 1A1

Abstract

A disparity gradient limit explains why the maximum amplitude of sinusoidal disparity gratings increases with decreasing disparity spatial frequency. It also explains why the largest disparity for binocular fusion (diplopia threshold) varies directly with stimulus element separation. Does a disparity gradient limit also apply to the detection of cyclopean shape? A previous study addressed this question and concluded that it does not. We examined this question by measuring the largest disparity amplitude (d_{max}) at which observers could judge the shape of cyclopean disparity gratings. We used trapezoidal, triangular, sinusoidal, and square wave gratings in order to dissociate the effects of disparity gradient and disparity spatial frequency. Gabor micropatterns were used to minimize potential scale-dependent interactions with luminance processing. Our results support a disparity gradient limit for cyclopean shape perception, with additional factors being involved at high disparity spatial frequencies. Combining the gradient limit hypothesis with lowpass disparity filtering describes the pattern of d_{max} for both smooth and discontinuous surface shapes. © 2000 Elsevier Science Ltd. All rights reserved.

Keywords: Stereopsis; Disparity spatial frequency; Disparity gradient limit; Disparity stage filters; Discontinuous surface shapes

1. Introduction

Stereopsis provides a major advantage to vision since it allows the identification of an object's surface shape from disparity information alone. How is the maximum disparity for perceiving stereo shape determined by *global* factors, that is, the pattern of disparity changes within the stimulus? Previous studies have identified at least two potentially important global factors: disparity spatial frequency and disparity gradient. We address here which of these is the critical factor.

Disparity spatial frequency was identified as an important factor by Tyler (1974) who modulated the disparities of sets of random dots sinusoidally. The modulation spatial frequency varied vertically, while the amplitude varied horizontally, and observers indicated the range in both dimensions for seeing depth. Tyler found that the maximum useful disparity decreased linearly with spatial frequency, which was ex-

plained by '…a limit in rate of change of disparity …'. Although the results could have been interpreted as an effect of stimulus size (of each half-cycle of the disparity grating), Tyler and Julesz (1980) showed otherwise. They varied the width of a rectangular portion of a dynamic visual noise field while keeping its height constant. All dots within the rectangle had either crossed or uncrossed disparities, and observers judged whether the rectangle was nearer or farther from fixation. The maximum useful disparity did not vary as a function of size linearly, and this suggested that for sinusoidal disparity gratings it was determined by some other factor.

Furthermore, Burt and Julesz (1980) reported that a *disparity gradient limit*, a unitless perceptual constant, determines the largest useful disparity for binocular fusion (the diplopia threshold). With their stimuli, each eye saw pairs of dots arranged in a regular grid. Disparities were identical within each stimulus but varied among stimuli. Within each eye's view, dot-pair separation was the same horizontally but varied vertically with the largest at the top. Observers indicated the row

* Corresponding author. Fax: + 1-514-843-1691.
E-mail address: zieg@vision.mcgill.ca (L.R. Ziegler)

below which fusion was impossible. Because the minimum dot-pair separation was found to be proportional to disparity, Burt and Julesz concluded that binocular correspondence cannot occur when the disparity gradient exceeds a critical value of about 1. Inherent constraints on correspondence based upon a gradient seem plausible, because the geometry of binocular viewing of opaque surfaces does not allow for a disparity gradient greater than 2 (Trivedi & Lloyd, 1985; reviews in Tyler, 1991; Howard & Rogers, 1995).

The disparity gradient limit hypothesis as applied to the identification of cyclopean surface shape however has recently been challenged. Lankheet and Lennie (1996) measured the ability of observers to detect sinusoidal disparity gratings in moving random dot displays that were degraded by various amounts of disparity dot noise. Both grating amplitude and frequency were varied to cover a large range. Lankheet and Lennie concluded that there was no evidence of a disparity gradient limit, stating that 'detection of binocular correlation depends on both spatial frequency and amplitude of disparity modulations, and cannot be reduced to a description in terms of gradient limits'.

Furthermore, the gradient limit hypothesis is inherently limited, since it does not predict the maximum disparity for discontinuous shapes. For example, a square wave disparity grating contains infinitely large gradients, so a gradient limit would imply shape would never be perceived, but it is. One may argue that square wave disparity gratings provide multiple surfaces, and thus are an exception to the gradient limit rule. Square wave gratings however do not always appear as multiple surfaces. If square gratings are not exceptional, how then can a gradient limit apply?

The present study addressed the effects of global factors, particularly disparity gradient and disparity spatial frequency, on the maximum disparity amplitude in the stimulus that allowed observers to see cyclopean shape, which for brevity we call d_{max}.[1] We used disparity gratings formed from random arrays of identical Gabor micropatterns, similar to the stimuli used in our study of stereoacuity, or d_{min} (Hess, Kingdom & Ziegler, 1999). There we found that high luminance spatial frequencies supported a greater range of disparity spatial frequencies than low luminance spatial frequencies. This suggested the possibility of interactions between the luminance and disparity domains for d_{max}. Previous studies have used broadband elements (e.g. Tyler, 1974; Lankheet & Lennie, 1996; Glennerster, 1998). Here we used a relatively narrowband stimulus, fixed in luminance spectral content, allowing us to examine global factors while avoiding potential interactions between luminance and disparity processing.

A number of different techniques have been used to measure d_{max}, and each type of experimental procedures has its own set of difficulties. In particular, it has been demonstrated that conclusions derived from experiments where a single element is judged near or far from the fixation plane do not necessarily generalize to cyclopean shape perception (Ziegler & Hess, 1999). Furthermore, measurements of d_{max} in terms of fusion limits may be complicated because of hysteresis, eye movements, or how fusion, rivalry, or diplopia is defined, as well as by variations in criteria among and between observers. We avoided these difficulties with a two-alternative shape perception task whereby, upon each trial, observers judged the orientation of a briefly presented disparity grating, as left or right oblique. As the disparity amplitude gradually increased, at some peak disparity, shape could not be perceived, and orientation discrimination fell to chance. We used disparity gratings with various cross-sectional shapes over a range of frequencies (here, *frequency*, *grating*, and *gradient* will be used in regard to the disparity domain, unless noted otherwise).

We have examined which global factor determines d_{max}, whether it is frequency, a gradient limit, a combination of the two, or perhaps some other factor. To do so we adopted the approach of Campbell, Johnstone and Ross (1981) to the analogous question for contrast sensitivity. That is, for each of a wide range of frequencies, we used different trapezoidal[2] grating shapes that allowed us to vary frequency and gradient independently. For these stimuli, a specific pattern of results would be expected, depending upon whether d_{max} is determined by a gradient limit or by frequency. The different predictions are shown in Fig. 1 where, for d_{max} as a function of ramp width, each segment represents the results for each of the grating shapes at a single frequency. D_{max} is expected to show a direct dependence (A) irrespective of frequency if gradient is the main factor. On the other hand, if frequency is the main factor d_{max} should be relatively invariant with ramp width, but dependent on frequency (B). Part of this work has been presented in abstract form (Ziegler, Hess & Kingdom, 1998).

2. Methods

2.1. Subjects

The three authors served as observers. Each had participated in previous stereo experiments and had normal or corrected-to-normal visual acuity and normal stereopsis. Data for the trapezoidal, including triangular, gratings were collected only from LZ and FK.

---

[1] Other researchers have used d_{max} to refer to the disparity that results in the greatest perceived depth (e.g. Tyler & Julesz, 1980).

[2] One may include triangular gratings as a special case of trapezoids (plateau width of zero).
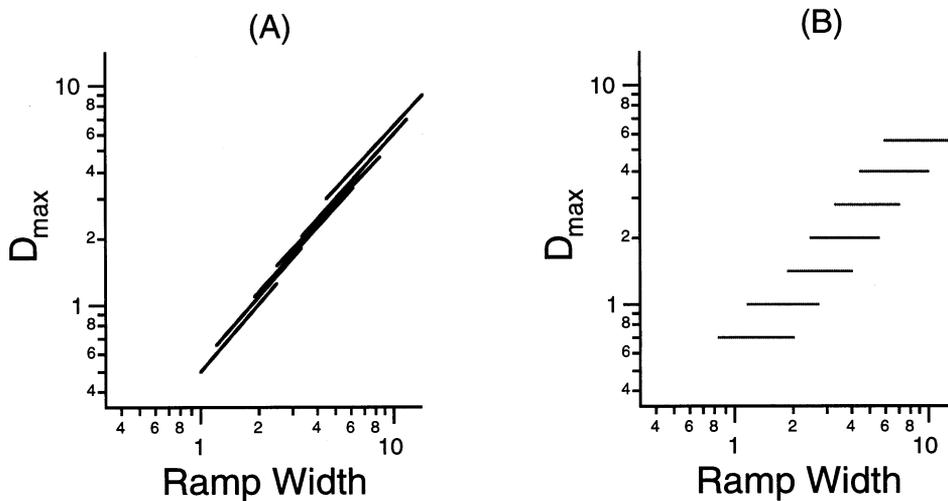
Fig. 1. Two possible outcomes for our experiment that measured the maximum disparity amplitude (d_{max}) of trapezoidal gratings as a function of ramp width, for combinations of frequency and shape. (A) If d_{max} is determined by a disparity gradient limit alone, and (B) if d_{max} is determined by disparity spatial frequency alone. Each segment represents d_{max} values for all shapes and one disparity spatial frequency.

2.2. Apparatus

All stimuli were generated using a Silicon Graphics O2 and displayed on a Sony GDM-20E21 monitor. Observers wore LCD shutter-glasses (StereoGraphics Inc. 'CrystalEyes') synchronized to alternations of the full-screen stereo half-images, so that each eye received a flicker-free image at 60 Hz. The linearity of the monitor was confirmed photometrically.

2.3. Viewing conditions

Observers sat at a viewing distance of 57 cm and ambient room illumination was low. The display subtended $28 \times 36°$ at a resolution of 1024×1280 pixels. The mean stimulus luminance was 6.0 cd/m², measured through a lens of the shutter glasses.

2.4. Stimuli

Each stereo half-image consisted of a random array of Gabor micropatterns ('Gabors'), with a Gaussian scale factor (σ) of 0.18° (perceptually 0.5° wide). Their carriers were in sine phase and at a center luminance spatial frequency of 1.68 c/deg. Luminance levels were assigned with subpixel accuracy. Each Gabor stereopair was positioned randomly. To prevent the introduction of occlusion artifacts when Gabors fell on top of one another, the pixel gray-levels of each Gabor, having zero baseline, were added first to an image buffer, with the background gray-level added last (Hess et al., 1999). We modulated the disparities of the Gabors at a particular spatial frequency to produce a disparity grating (example, Fig. 2). The disparity grating was oriented at $\pm 26°$ from horizontal. To be sure that a

response could not be based upon the depth seen at a single location, we assigned the modulation phase at random for each trial.

We designated the trapezoidal and triangular grating shapes following Campbell et al. (1981) by their half ramp width t in radians. They were a triangular waveform ($t = \pi/2$), a thin trapezoid ($\pi/4$), and a nearly square trapezoid ($\pi/8$). The thin trapezoid is shown in Fig. 2. For a single corrugation frequency, as t approaches 0, the stereo shape becomes more square-like. For each shape, seven frequencies were used, from 0.044 to 0.35 c/deg ($\lambda = 23–3°$).

A potential monocular cue for detecting the corrugations of non-horizontal gratings is a difference in element density, i.e. compression along slopes, and rarefaction at peaks and troughs. We found this cue however to be insufficient to perform our task at the disparities reported here-if it had been, the staircase would have failed to converge. On the rare occasions when this cue became visible, that staircase was aborted and its data ignored.

A 1° wide central cross was present whenever the stimulus was not displayed. Exposure duration was 117 ms (14 stereo frames), well below saccadic latencies (Rashbass & Westheimer, 1961; Stevenson, Cormack & Schor, 1994). Immediately after stimulus presentation, but before user response, the vertical arms of the cross became nonius lines. They were used to confirm that, with the brief presentations, fixation was easy to control.

2.5. Procedure

A single grating was presented on each trial, and observers used the mouse buttons to report the orienta-
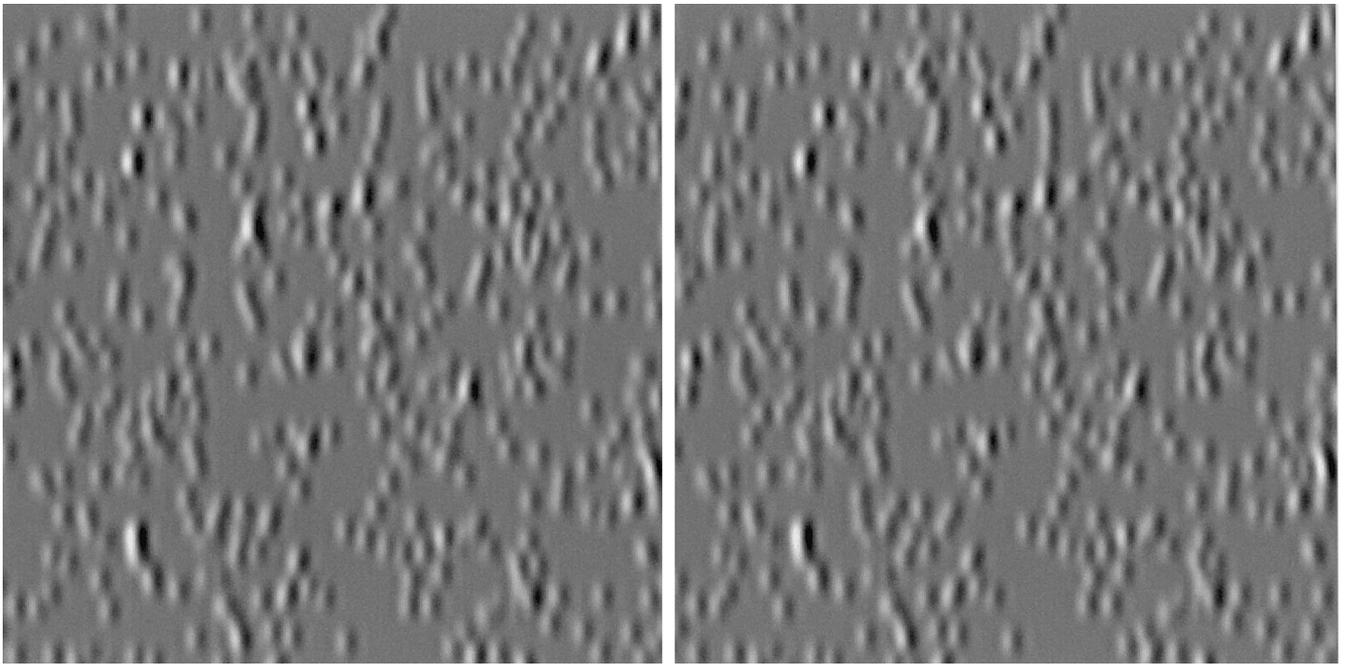
Fig. 2. A stereogram of an obliquely oriented disparity grating created from many Gabor elements. Observers discriminated between oblique orientations of similar gratings of various shapes and spatial frequencies. This shape is the thin trapezoid. All stimuli in this study were composed of identical Gabor elements: luminance spatial frequency, 1.68 c/deg; σ, 0.18°; contrast, 33%.

tion of the corrugation, left or right oblique. Disparity amplitude began at 20 min and was adjusted automatically by a conventional staircase procedure, i.e. increased after two consecutive correct responses and decreased after every incorrect response, each by one-quarter octave ($\sim 19\%$). After 12 reversals, the procedure terminated automatically. D_{max} was estimated as the geometric mean of the last eight reversals. These estimates are at the 71% correct level. We report the geometric means of these estimates from at least two, and generally four or more, staircases.

3. Results and discussion

For the trapezoidal gratings, which we used to vary gradient and frequency independently, recall how d_{max} would be expected to vary with each factor. When plotted against ramp width, as in Fig. 1A (in degrees of absolute visual angle while ignoring frequency and shape), if d_{max} were determined by a gradient limit alone, then values should fall on a straight line. The line would have a $+1$ slope and a location defined by the gradient limit, or g_{max}. On the other hand, following Fig. 1B, if d_{max} were determined by frequency alone, then the values would lie on separate, vertically displaced, horizontal lines (each line corresponding to one frequency and all shapes).

Fig. 3A shows d_{max} as a function of ramp width. A

distinct asymptote appears for the large ramp widths, as predicted by a gradient limit (Fig. 1A). For small ramp widths however the values are larger than predicted by the gradient limit hypothesis, and are in the direction of the frequency hypothesis. This may be explained by other factors however, as shown below. Results for sine gratings, obtained in the same manner (below), are included in the figure.[3] The dashed (coarse) line for each graph in Fig. 3A is the best fit constrained to a linear function (a slope of $+1$ in log space). These lines provide estimates of g_{max} of 1.5 for LZ and 2.4 for FK.

Fig. 4A shows the trapezoid data in terms of d_{max} versus frequency. The slopes are steepest for the triangles and become shallower as shape becomes more square-like. These differences, that are contingent upon shape, decrease with increasing frequency. Observer LZ provided control data (frequency, 0.25 c/deg) at a density of 4800 elements with identical results. This suggests that the differences between the shapes at that frequency were not the result of inadequate spatial sampling. The convergence of the different shape curves indicates that whatever distinguishes the shapes has progressively less effect as frequency is increased.

---

[3] As suggested by a reviewer, by estimating the effective ramp width of a sinusoid. We used the ramp widths of trapezoidal gratings, of the same frequency and amplitude as the sinusoids, that had the same maximum gradient, that is, $t = 1$.
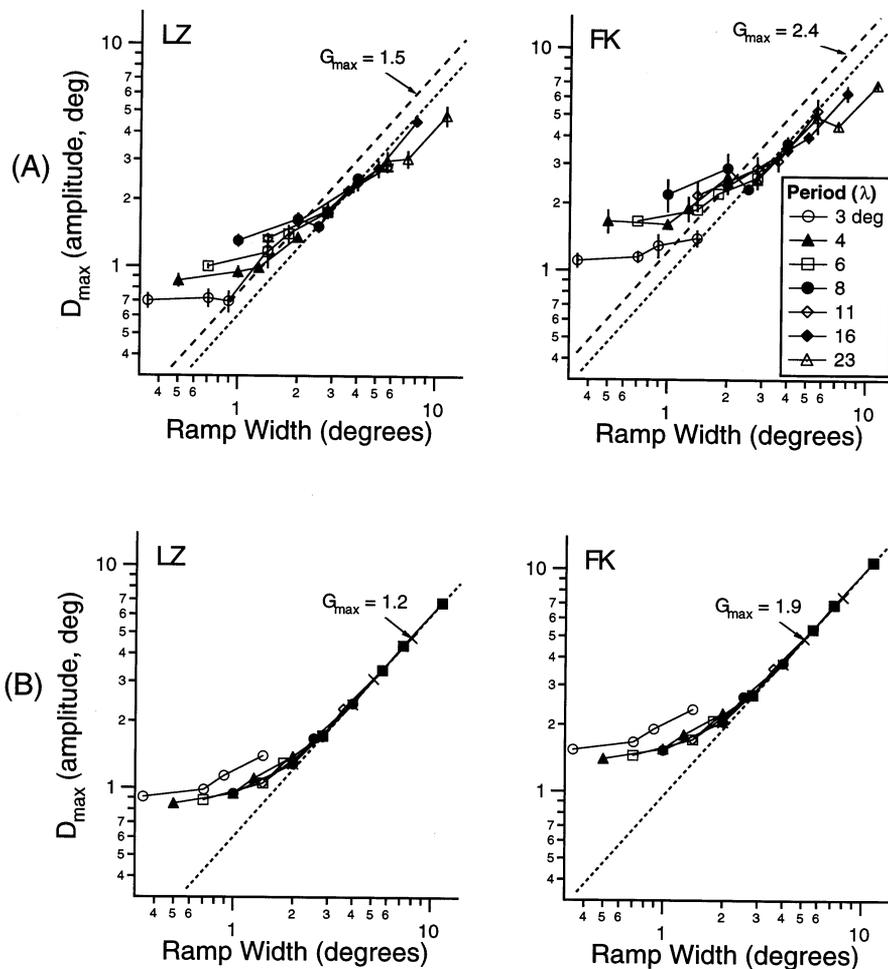
Fig. 3. (A) D_{max} for cyclopean shape perception as a function of ramp width (in degrees of absolute visual angle). Each isofrequency curve consists of measurements of d_{max} for four grating shapes in order of increasing ramp width, that is, left to right: $\pi/8$ (fat) trapezoid, $\pi/4$ (thin) trapezoid, sinusoid, and triangle. Error bars here and in subsequent graphs designate ± 1 SE. Broken lines are the best fits based upon a disparity gradient limit alone, i.e. constrained to a slope of $+1$ in logspace. (B) Simulation results (Section 3.4), plotted in the same manner, which used a simple model that included disparity domain lowpass filtering as well as a disparity gradient limit. Dotted lines in both (A) and (B) represent g_{max} from the simulation (1.2 for LZ and 1.9 for FK).

We next analyzed this convergence of the curves while taking into account the differences between the shapes in the frequency domain. The shapes are composites of a fundamental frequency and its odd harmonics, each at a specific amplitude. The amplitude of the fundamental Fourier component of a trapezoid is different than that of the trapezoid itself, as shown in Fig. 4 (right). In Fig. 4B we have recast the data in terms of the amplitude of the fundamental. At the lower corrugation frequencies these curves are separate, indicating that shape (i.e. gradient) determined d_{max} there. At 0.25 c/deg and higher however the harmonics that differentiated the shapes, starting with the third harmonic, appear to have had little effect. This analysis therefore points to an upper disparity spatial frequency limit somewhere between 0.3 and 0.8 c/deg. Indeed, we found that we were unable to perform our task with sine gratings above 1.0 c/deg, even after increasing the density to 9600 Gabors/screen.

3.1. Sinusoidal and square wave gratings

Under conditions identical to those with the trapezoidal gratings, we also measured d_{max} for sine and square gratings. Fig. 5A shows that for sine gratings, d_{max} decreased with increasing frequency for all three observers. We had included this data in Fig. 3A in plotting d_{max} as a function of ramp width. We calculated the g_{max} values at each frequency using the purely mathematical relation for sinusoids:

$$g_{max} = 2\pi f d_{max}$$

where f is frequency. This formula yielded values of g_{max} from our data that varied considerably, both between and within observers (0.7–3). Although our tasks were different and our stimuli covered a different range of disparity spatial frequencies, these results nevertheless are similar to those of Lankheet and Lennie (1996).
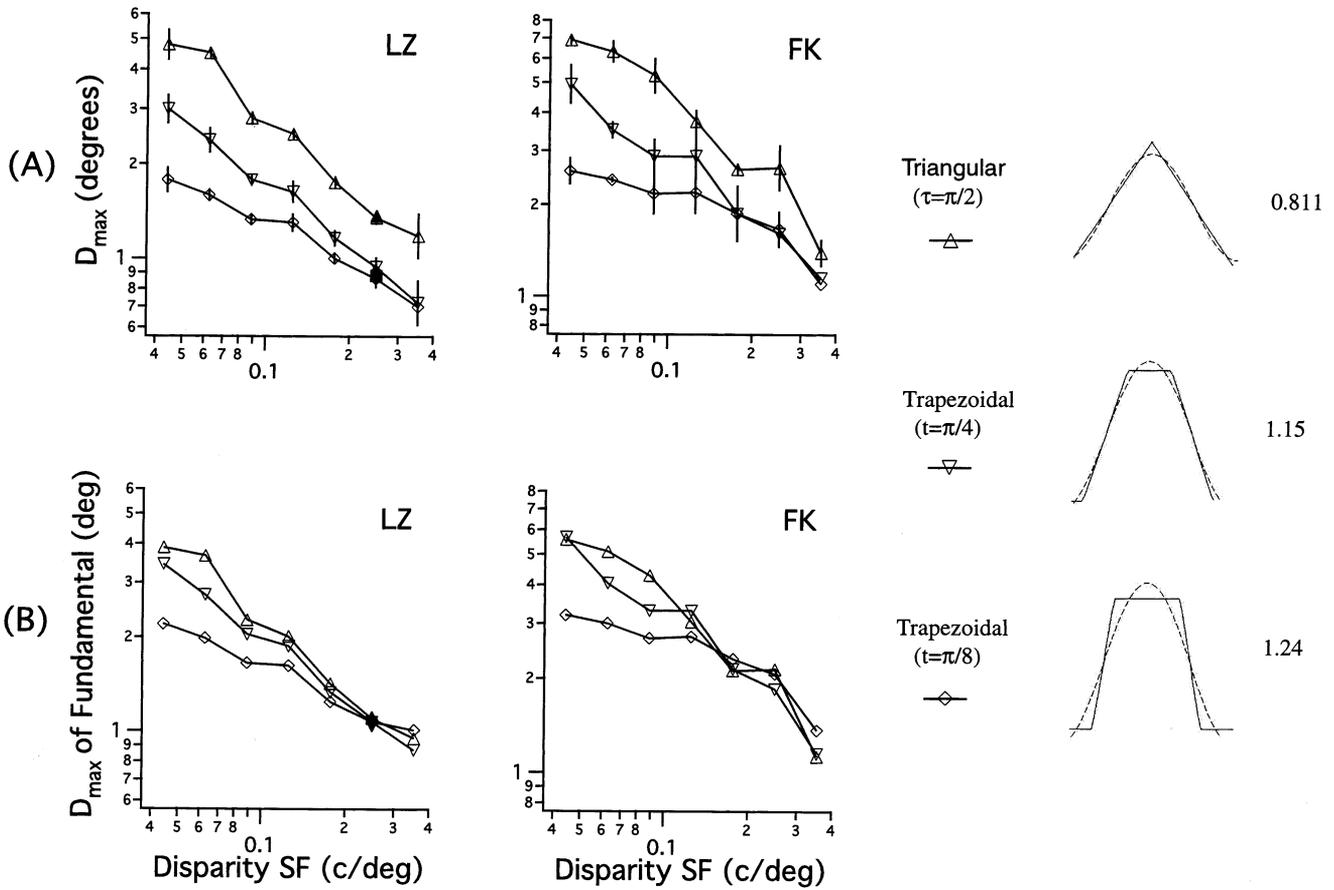
Fig. 4. (A) D_{max} for cyclopean shape perception as a function of disparity spatial frequency for the trapezoidal gratings. The filled symbols at 0.25 c/deg for LZ are from a control condition of four times the regular density. Slopes of best-fit lines were, top to bottom, -0.73, -0.68, and -0.45 for LZ, and -0.75, -0.66, and -0.36 for FK. (B) D_{max} of the fundamental Fourier component of each shape, from the same data, based upon the ratios (listed on the right) between the disparity profiles of each shape (shown as solid lines) and their fundamental components (dashed lines).
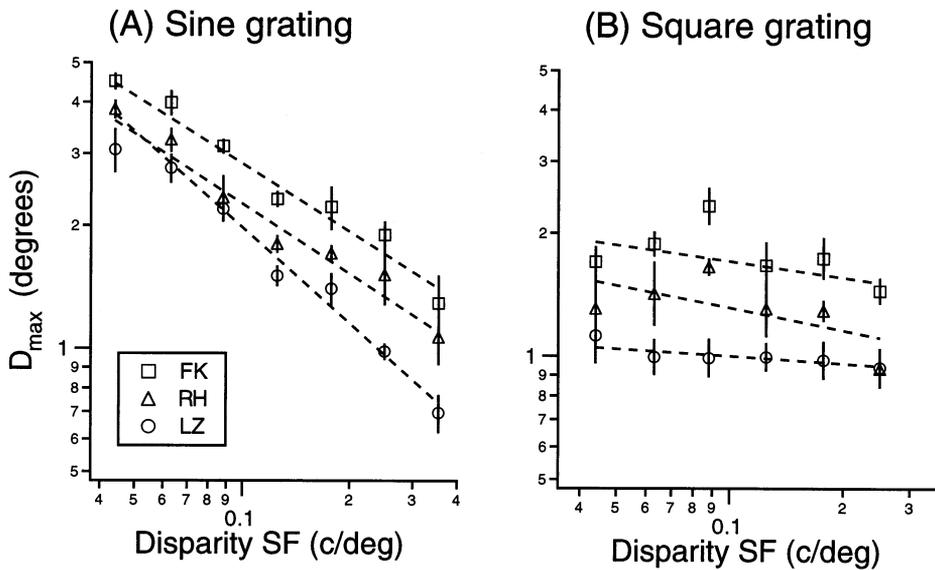

Fig. 5. D_{max} for cyclopean shape as a function of disparity spatial frequency for (A) sine, and (B) square wave gratings. Broken lines are from least squares fits and have slopes of -0.55, -0.57, and -0.78 for the sines, and -0.13, -0.18, and -0.06 for the square waves, for FK, RH, and LZ, respectively.
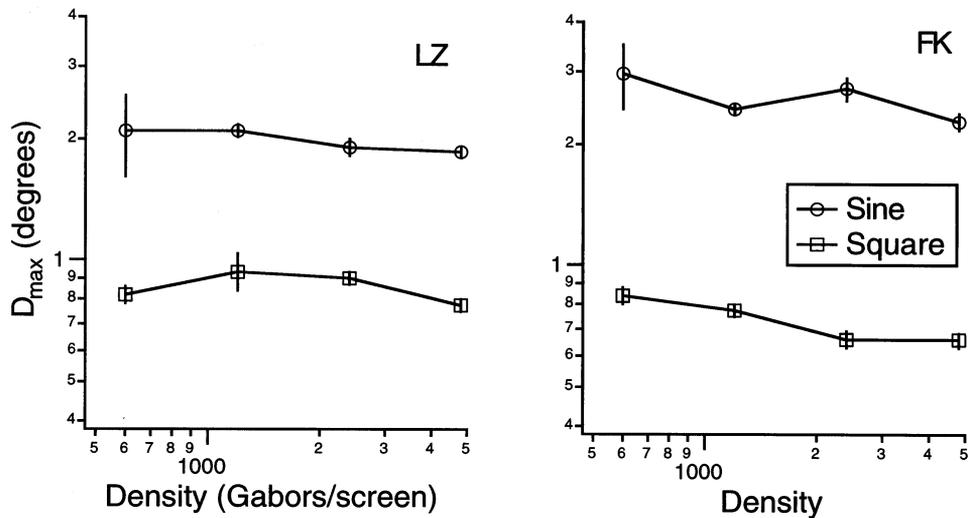
Fig. 6. D_{max} for cyclopean shape as a function of Gabor density. We used square wave and sinusoidal disparity gratings each at a disparity spatial frequency of 0.125 c/deg.

Using the largest values that they provided in their Fig. 9 of (frequency × amplitude), we calculated that their values of g_{max} ranged from about 0.5 to 2.

For square waves, Fig. 5B shows the function of d_{max} versus frequency. Compared to the sinusoid data, the functions are relatively constant.[4] In addition, we wanted to be sure that certain local factors, influenced by density, do not determine d_{max} for square waves. That is, although disparity gradient is normally considered independent of Gabor density, it may be assumed that there is some finite disparity gradient at edges, related somehow to the average distances between Gabors. Fig. 6 shows however that over a 3-octave (8 ×) change in element density, d_{max} for square gratings is independent of density.

Density also had little effect on d_{max} under the same conditions for sine gratings, as shown in Fig. 6. Similarly, Lankheet and Lennie (1996) found that density did not effect the detection of sine gratings over a range of frequencies, nor on the highest detectable frequency. In conclusion, the lack of an effect of density on d_{max} for either square or sine gratings confirms that the effects of gradient and frequency on d_{max} reported here are truly global.

3.2. Alternate explanations

We may safely discard a number of other explanations for our results. First is that d_{max} decreased with frequency for sinusoidal gratings because the number of Gabors within Panum's area decreased. Over a large range of densities however d_{max} for sine gratings as a function of

density was constant, as shown in Fig. 6.

Second is that disparity gradient appeared critical because it determined the width of the ramp that was enclosed by Panum's area. However, Burt and Julesz (1980) reached the exact opposite conclusion; namely, that Panum's area itself is determined by disparity gradient.

Third is that the decrease in d_{max} with frequency for sinusoids was because critical regions of the waveform were at larger eccentricities for lower frequencies, on average, because our gratings were presented with a random phase. If that were the case however then d_{max} for square gratings would also be expected to have decreased with increasing spatial frequency, and this was generally not found, as shown in Fig. 5B.

Furthermore, we mentioned that Tyler and Julesz (1980) examined the hypothesis that the size of regions of constant disparity determines d_{max}, and they found a square-root dependence on a log–log plot. Our data also call this hypothesis into question. In Fig. 7, we show d_{max} plotted as a function of plateau width for those grating shapes that contained a well defined plateau, that is, the fat and thin trapezoids. To analyze these graphs, one must consider that while d_{max} appears to increase with plateau width, plateau width and ramp width were not independent factors. Instead, for a given waveform, as plateau width increased (with increasing spatial period), so did ramp width, allowing for a larger d_{max} based upon a disparity gradient limit. The data fall naturally into two lines, corresponding to the two shapes. This indicates that gradient actually determined d_{max}, because if plateau width determined d_{max}, all points would lie instead on a single line. For our task, the size of constant disparity regions within a shape does not determine d_{max}. Ramp width (gradient), not plateau width, therefore appears to be the critical factor.

---

[4] The frequency of 0.35 c/deg was not used for square gratings because there may have been a monocular cue at large disparities from the gap created by the displacement of Gabors in each half-cycle.

One possible criticism of this conclusion however is that our task may have been performed by using only the sloping portions of the gratings. At threshold we cannot say for certain which features were important. Perceptually however (and this applies to all the waveforms used in this study) the shapes increased in depth amplitude as disparity was increased until they abruptly and completely disappeared. That is, the sloping regions did not appear alone.

3.3. Why is a gradient limit model so poor at small ramp widths?

Why does the gradient limit hypothesis predict smaller values of d_{max} for the small ramp widths (at the high frequencies) as shown in the lower left portion of Fig. 3A? There are a number of possible explanations. It may be related to our upper frequency cutoff being lower than that found by Tyler (1974) who, using broadband random dot displays, found it to be about 3–4 c/deg. We have shown previously that the upper disparity spatial frequency cutoff is dependent upon luminance spatial frequency (Hess et al., 1999). Thus, the flattening of the curve in Fig. 3A may be because of the specific *center luminance spatial frequency* of our narrowband stimuli. As a control, we tried using stereograms consisting of closely packed grids of the Gabors. Absolute disparities were constant (10 min) but alternated by row in sign. We measured the highest frequency (by varying grid spacing) that allowed our observers to see the square wave shape, yielding about 1.8 c/deg for all three observers. This suggests that the upper frequency limit was not the only factor responsible for the flattening of the curves in Fig. 3A.

A second possible factor is *disparity averaging* (Howard & Rogers, 1995), because our Gabors occasionally overlaid one another. To estimate the possible contribution of disparity averaging, we measured the minimum distance between two of the Gabors that resulted in their appearance at separate depths. The displays were identical to the ones used in our main experiments except the Gabors were arranged in a grid pattern, with a horizontal step edge of ($\pm$) 10 min disparity passing through the center of the display. As we brought Gabors on either side of the step edge closer together, their apparent depth did not begin to merge until their center separation was 0.20° or less. This suggests an upper frequency limit of about 2.5 c/deg from disparity averaging. Although this is higher than the limit suggested by the results of the main experiment, we cannot rule out an influence of disparity averaging.

A third possibility is that our 0.5° wide Gabors were flat, so would have represented the sinusoidal surface shape more poorly as frequency increased. This might have acted in effect as a disparity filter.

3.4. A simple simulation

Our results can be described by a model that combines a disparity gradient limit with lowpass filtering, or blurring, in the disparity domain. The model explains the higher-than-expected d_{max} values at small ramp widths, which in the previous section we suggested were caused by a number of possible factors. The model accounts for the convergence of the functions of d_{max} versus frequency at high frequencies for all shapes, as well as the different slopes of those functions. In addition, it addresses the problem of square wave gratings, where d_{max} did not vary with frequency. Because the step edges of square waves are the same regardless of frequency, if filter size were small relative to grating period, then filter size alone would determine d_{max}. Then d_{max} would be constant as a function of grating frequency, as we found.
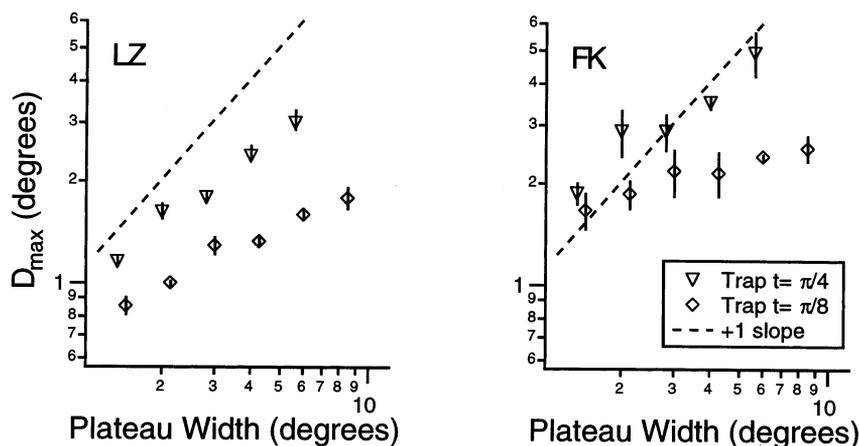

Fig. 7. D_{max} for cyclopean shape as a function of plateau width. Values would fall on a single line if the size of the region of constant disparity determined d_{max}. They naturally group into two lines according to grating shape, as expected if disparity gradient determined d_{max}.
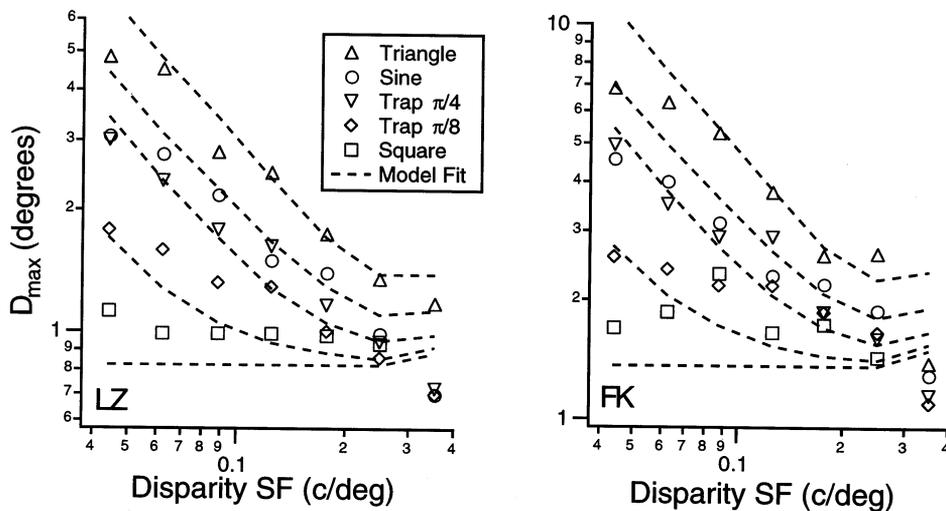
Fig. 8. Simulation results (broken lines) compared with our empirical measurements (symbols) of stereo shape d_{max}. The simulation used two free parameters: a disparity gradient limit, and a disparity lowpass filter size (Section 3.4). The curves are in the same order, top-to-bottom, as the legend symbols (top-to-bottom), as well as the general trend in the data.

A computer program provided the best fit to our empirical d_{max} values for all shapes and frequencies, based upon two free parameters: σ and g_{max}. The first parameter, σ was the scale factor of the Gaussian blurring function with which a 1-D vector representing each stimulus waveform was first convolved. The amplitude of the resultant waveform was then adjusted so that its maximum disparity gradient was equal to the second parameter, g_{max}, and that amplitude became the estimate of d_{max}. Iterating with this routine, our simulation was able to find a single pair of σ and g_{max} that fitted best the empirical values of d_{max} for all shapes and all frequencies. The procedure used the multivariate function minimization routine in MatLab (Nelder–Mead simplex method), so both σ and g_{max} could be adjusted simultaneously. We confirmed the existence of a unique, optimum solution pair by using a separate program that plotted the sums-of-squares function over the useful range of the two parameters. This function varied smoothly and was without multiple local minima.

Using the data from all five shapes, the simulation provided reasonably good fits, with χ^2 of 2.2 and 5.8 for LZ and FK, respectively (d.f. = 33, $P < 0.005$). The fits explain 97 and 95% of the variance in the data, as estimated using r^2, the coefficient of determination. These fits were better than those provided by the gradient-only model, represented by the dashed lines in Fig. 3(A), where χ^2 was 7.3 and 15.0 (d.f. = 26, $P < 0.05$). (excluding the square wave data; otherwise, a d_{max} of 0 is predicted, resulting in an infinite χ^2). The gradient-only fits had $r^2 = 0.95$ and 0.93 without, and $r^2 = 0.90$ and 0.86 with, the square wave data. Fig. 3B shows the estimates d_{max}, including the sinusoid data plotted as a function of ramp width in the same manner as the

empirical data in Fig. 3A. Our model yielded estimates of σ of 0.55 and 0.57° (about three times the Gabor σ), and g_{max} of 1.2 and 1.9 for LZ and FK. The results were consistent regardless of the portion of the data used in the fit. For example, when only the sine and square wave data were used for the fits, σ were 0.67 and 0.78°, and g_{max} were 1.2 and 1.9. Similar values were also obtained by using only the trapezoid and triangle data, where σ were 0.57 and 0.90°, and g_{max} were 1.4 and 1.8. These values for g_{max} are reasonably close to those reported by Burt and Julesz (1980), and to the values of 0.9 and 1.9 that we calculated from the data fits in Tyler (1974). These values of g_{max} are also close to those used in models (Pollard, Mayhew & Frisby, 1985) and are consistent with constraints based upon the geometry of binocular viewing (Trivedi & Lloyd, 1985).

Although a model with more free parameters might provide better fits to our results, Fig. 8 shows that this relatively simple model captures the main qualitative trends in the data (dashed curves), though not the precise individual estimates of d_{max}. The order of the location of the five curves is preserved, and the curves also converge with increasing disparity spatial frequency. The results of the simulation were disappointingly poor however for the highest disparity spatial frequencies where its d_{max}'s were too large. A more elaborate model might avoid this problem if it completely omitted disparity filters above some limiting frequency.

For square disparity gratings, this simulation resulted in a function of d_{max} versus frequency that was nearly constant for both observers. This compares favorably with our empirical data (Fig. 6). Thus, the disparity filter hypothesis may explain how a gradient limit applies to square gratings.

In conclusion, by using a variety of grating shapes, we have demonstrated the importance to shape-from-stereo of a disparity gradient limit. Clearly, however, other factors may influence d_{max} especially near the cyclopean upper frequency limit, and for square waves.

Acknowledgements

References

Burt, P., & Julesz, B. (1980). Modifications of the classical notion of Panum's fusional area. *Perception*, *9*(6), 671–682.

Campbell, F. W., Johnstone, J. R., & Ross, J. (1981). An explanation for the visibility of low frequency gratings. *Vision Research*, *21*, 723–730.

Glennerster, A. (1998). d_{max} for stereopsis and motion in random dot displays. *Vision Research*, *38*(6), 925–935.

Hess, R. F., Kingdom, F. A. A., & Ziegler, L. R (1999). On the relationship between the spatial channels for luminance and disparity processing. *Vision Research*, *39*(3), 559–568.

Howard, I. P., & Rogers, B. (1995). *Binocular vision and stereopsis*. New York: Oxford University Press.

Lankheet, M. J. M., & Lennie, P. (1996). Spatio-temporal requirements for binocular correlation in stereopsis. *Vision Research*, *36*(4), 527–538.

Pollard, S. B., Mayhew, J. E. W., & Frisby, J. P. (1985). PMF: A stereo correspondence algorithm using a disparity gradient limit. *Perception*, *14*, 449–470.

Rashbass, C., & Westheimer, G. (1961). Disjunctive eye movements. *Journal of Physiology* (*London*), *159*, 339–360.

Stevenson, S. B., Cormack, L. K., & Schor, C. M. (1994). The effect of stimulus contrast and interocular correlation on disparity vergence. *Vision Research*, *34*, 383–396.

Trivedi, H. P., & Lloyd, S. A. (1985). The role of disparity gradient in stereo vision. *Perception*, *14*, 685–690.

Tyler, C. W. (1974). Depth perception in disparity gratings. *Nature*, *251*, 140–142.

Tyler, C. W., & Julesz, B. (1980). On the depth of the cyclopean retina. *Experimental Brain Research*, *40*, 196–202.

Tyler, C. W. (1991). Cyclopean vision. In: D. Regan, *Vision and visual dysfunction*, *vol. 9: Binocular vision* (pp. 38–71). Boca Raton, FL: CRC Press.

Ziegler, L. R., & Hess, R. F. (1999). Stereoscopic depth but not shape from second-order stimuli. *Vision Research*, *39*(8), 1491–1507.

Ziegler, L. R., Hess, R. F., & Kingdom, F. A. A. (1998). Factors that determine d_{max} for shape-from-stereo. *Perception* (*Suppl*), *27*, 109b.